Harvesting Broadband Kinetic Impact Energy from Mechanical Triggering/Vibration and Water Waves

Xiaonan Wen,[†,⊥] Weiqing Yang,[†,‡,⊥] Qingshen Jing,[†] and Zhong Lin Wang[†,§,*]

[†]School of Materials Science and Engineering, Georgia Institute of Technology, Atlanta, Georgia 30332-0245, United States, [‡]Key Laboratory of Advanced Technologies of Materials (Ministry of Education), School of Materials Science and Engineering, Southwest Jiaotong University, Chengdu 610031, China, and [§]Beijing Institute of Nanoenergy and Nanosystems, Chinese Academy of Sciences, Beijing, China. [⊥]X. Wen and W. Yang contributed equally to this work.

ABSTRACT We invented a triboelectric nanogenerator (TENG) that is based on a wavy-structured Cu–Kapton–Cu film sandwiched between two flat nanostructured PTFE films for harvesting energy due to mechanical vibration/impacting/compressing using the triboelectrification effect. This structure design allows the TENG to be self-restorable after impact without the use of extra springs and converts direct impact into lateral sliding, which is proved to be a much more efficient friction mode for energy harvesting. The working mechanism has been elaborated using the capacitor model and finite-element simulation. Vibrational energy from 5 to 500 Hz has been harvested, and the generator's resonance frequency was determined to be ~100 Hz at a broad full width at half-maximum of over 100 Hz, producing an open-circuit voltage of up to 72 V, a short-circuit current of up to 32 μA, and a peak power density of 0.4 W/m^2. Most importantly, the wavy structure of the TENG can be easily packaged for harvesting the impact energy from water waves, clearly establishing the principle for ocean wave energy harvesting. Considering the advantages of TENGs, such as cost-effectiveness, light weight, and easy scalability, this approach might open the possibility for obtaining green and sustainable energy from the ocean using nanostructured materials. Lastly, different ways of agitating water were studied to trigger the packaged TENG. By analyzing the output signals and their corresponding fast Fourier transform spectra, three ways of agitation were evidently distinguished from each other, demonstrating the potential of the TENG for hydrological analysis.

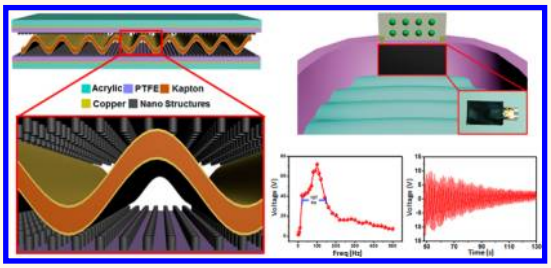

KEYWORDS: triboelectric · electrostatic · generator · broadband · mechanical energy · water wave energy

With fossil fuels running out and the safety of nuclear power being harshly debated, the arguably best option to relieve or even solve humans' energy issues is to harvest green energy from our vast environment.[1−3] With the exception of solar power, all the rest of major green energy harvesting ultimately depends on the use of electromagnetic generators, which is the most traditional technology for converting mechanical energy into electricity. On one hand, this indicates that an electromagnetic generator is superior in many aspects; on the other hand, our sole dependence on this type of generator may also lead to many limitations. Shortcomings of electromagnetic generators include high cost, poor portability, heavy weight, inefficiency at low triggering frequencies, and incompetence at collecting minor mechanical energy of different triggering actions in the environment. Therefore, it is necessary and beneficial to study and develop other types of electric generators to compensate for the above shortcomings.

Triboelectrification is a process of charge separation and transfer between two materials through mechanical contact and friction.[4−6] As an effect that has been known for thousands of years, much earlier than the electromagnetic effect, its potentials for electric generation were not very well explored until recently.[7,8] Thanks to a number of works reported in the last two years with the use of polymer and nanostructured materials, the output level of triboelectric nanogenerators (TENGs) has been drastically increased.[9−12] Although the original purpose of developing TENGs was to power nanodevices or small electronics, we now see a realistic chance of using this technology for large-scale energy harvesting, simply because of its cost-effectiveness, easy

* Address correspondence to zlwang@gatech.edu.

Received for review May 13, 2014 and accepted June 16, 2014.

Published online June 25, 2014
10.1021/nn502618f

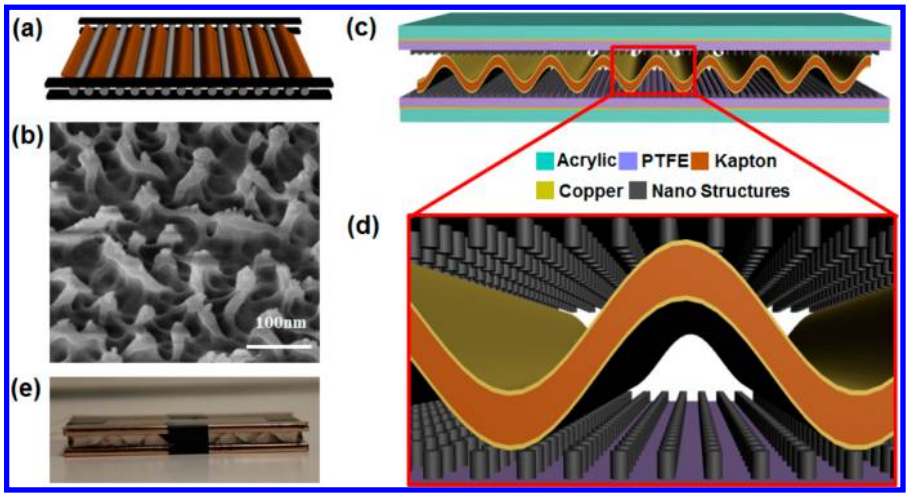

Figure 1. (a) Schematic of the method to fabricate wavy Kapton films. (b) SEM image of the ICP-processed PTFE film surface. (c) Schematic of the device structure. (d) Magnified schematic of the device, showing that the wavy core is in periodical contact with the nanostructures on the PTFE films. (e) Photograph of an as-fabricated TENG device before packaging.

fabrication, high efficiency, high power density, light weight, easy scalability, and diverse formats of mechanical triggering.[5] With the proper design, TENGs can be efficient for collecting mechanical energy in both the low- and high-frequency range, at both small and large scale. Therefore, TENGs can have significant advantages over electromagnetic generators under certain circumstances.

We believe that a significant source of future green energy is from the ocean, but such huge energy is hugely underexplored due to the lack of technologies. It is estimated that, if well utilized, wave energy may provide 10% of today's global energy consumption.[13] For the U.S. alone, the total amount of ocean wave energy resource is estimated to be 2.6 PWh/yr,[14,15] while the total amount of wind energy resource is estimated to be 10.8 PWh/yr.[16] With their potentials on the same scale, in 2011, wind power production in the U.S. was at 120.5 TWh,[17] while ocean wave power production was trivial.[13] Although efforts in utilizing ocean wave energy could be dated back to 1890,[13] there has not been any commercial wave power farms up to now. This situation is due to several challenges from using the electromagnetic generator system such as low turbine efficiency at ocean wave frequency, seawater erosion of facilities, heavy weight, and the high cost of equipment maintenance and replacement. Considering that TENGs have obvious advantages over electromagnetic generators in all these challenging aspects, this type of generator may become the solution that allows us to finally tap into the huge potential of ocean wave energy.

In this work, we report a TENG with a wavy-structured Cu–Kapton–Cu sandwiched between two flat nanostructured PTFE films. This structure design allows the TENG to be self-restorable after impact without the use of extra springs and also converts direct impact into lateral sliding, which is proved to be a much more efficient friction mode for energy harvesting.[18,19] Nonlinear factors in the wavy core's stiffness allow the TENG to be efficient at collecting mechanical energy over a very broad frequency range.[20−22] The light weight and high flexibility of the device itself ensure that the generator is able to collect minor impacts from the environment in addition to major ones. Most importantly, by water-proof packaging of the TENG, collection of water wave energy was successfully demonstrated, showing potentials of the TENG technology for harvesting the vast but barely utilized ocean wave energy resources. Lastly, different ways of water agitation were studied to trigger the packaged TENG. By analyzing the output signals and their corresponding fast Fourier transform (FFT) spectra, three agitation methods were distinguished from each other, demonstrating the potential of the TENG for hydrological analysis.

RESULTS AND DISCUSSION

Details of the device fabrication are stated in the Methods section. Specifically, a set of metal rods (with a diameter of 1/4 in.), as shown in Figure 1a, was used to assist with the fabrication of the wavy-structured core. PTFE films were processed with inductively coupled plasma (ICP) etching[23,24] to produce the nanostructures shown in Figure 1b, which would largely enhance contact electrification.[18,25,26] The device structure is schematically shown in Figure 1c, accompanied by a magnified schematic in Figure 1d and a picture of a real device in Figure 1e. The length and width of the TENG here is 10 and 5 cm, respectively, and the cost for such a device is estimated at around $1. The size of the device could be easily scaled up for large-scale applications.

Figure 2a shows the cross section schematic of the TENG. Once the acrylic substrate is under impact, the wavy core will be compressed in the vertical direction and be extended in the horizontal direction,

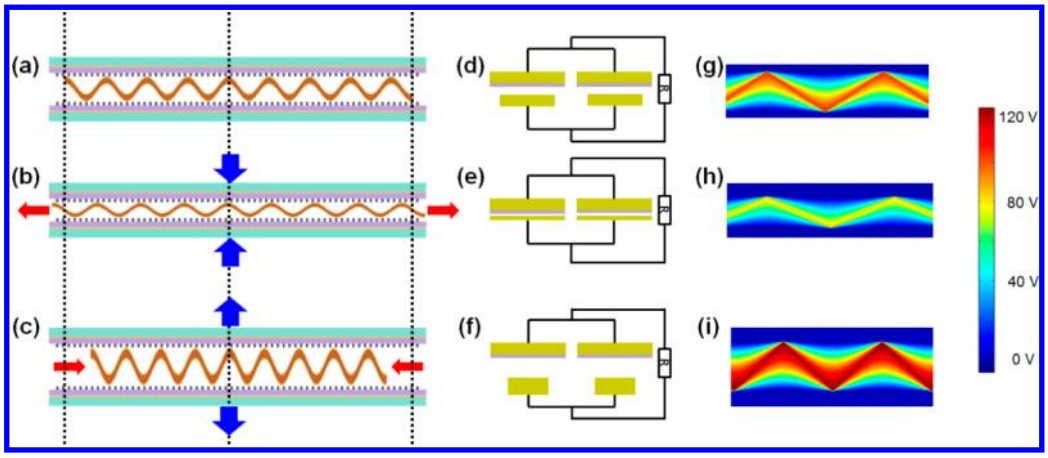

Figure 2. Description of the TENG's working mechanism. Cross sectional schematics of the device in the (a) balanced state, (b) compressed state, and (c) released state. Equivalent circuit of the device in the (d) balanced state, (e) compressed state, and (f) released state. Finite-element simulation of the potential distribution in the device in the (g) balanced state, (h) compressed state, and (i) released state.

converting the vertical compressing force into lateral friction between the core and both PTFE surfaces, as shown in Figure 2b. Also the contact area between the PTFE and Cu film is increased, and the average distance between the two is reduced. Once the impact is removed, the wavy core will retract in the horizontal direction and extend in the vertical direction, also leading to lateral friction between the core and both PTFE surfaces, as shown in Figure 2c. Also the contact area between the PTFE and Cu film is reduced, and the average distance between the two is increased. The working process of the TENG includes two parts: the charge transfer and charge separation. The transfer is accomplished by the lateral friction between the copper thin films, which lose electrons, and the PTFE films, which gain electrons. The charge separation process is accomplished by the change of capacitance between the copper coated on the Kapton film and the copper coated on the back side of the PTFE films. Our TENG device could be considered as two capacitors connected in parallel, as shown in Figure 2d. The purple layers under the top electrodes represent the PTFE films that carry negative static charges as generated due to the triboelectrification between PTFE and Cu. These negative static charges induce positive charges on both the top and the bottom electrodes. Under impact, the distance between the two electrodes is decreased and the area of the bottom electrodes (corresponding to the projected area of the wavy core) is increased, as shown by Figure 2e. Consequently, more positive charges are induced on the bottom electrode and fewer on the top electrode, leading to current flow in the external circuit. When the impact is removed, the distance between the two electrodes is increased and the area of the bottom electrodes is decreased, as shown by Figure 2f. Consequently, fewer positive charges are induced on the bottom electrode and more on the top electrode, leading to current flow in the opposite direction in the external circuit. This is the general working mechanism of our TENG. By assigning a fixed amount of charges onto the PTFE and using finite-element simulation, we obtain the electric field potential distribution of the three cases shown in Figure 2g, h, and i, respectively. Consistent with our explanation above, with fixed amount of Q, the change in capacitance leads to a change in the field potential that consequently drives the electrons to flow in the external circuit.

To measure the output performance of our TENG, we mounted the device onto an electrodynamic shaker that could provide vibration at a fixed amplitude and tunable frequencies. Open-circuit voltage and short-circuit current were measured by directly connecting the TENG to a Keithley 6514 electrometer. Measurements were performed from the frequency of 5 to 500 Hz. Sample voltage output at 5 Hz is shown in Figure 3a (a1), with an average peak voltage of 4.2 V. Sample voltage output at 100 Hz is shown in Figure 3a (a2), with an average peak voltage of 72 V. This is significantly larger than the output under 5 Hz even though the same amplitude was used. When the vibration frequency was increased to 500 Hz, however, we see a drop in the output peak voltage, averaged at 7.5 V, as shown in Figure 3a (a3). The corresponding current output was also measured, selectively shown in Figure 3b (b1−b3). Average peak current output was 3.3 μA at 5 Hz, 31 μA at 100 Hz, and 5.2 μA at 500 Hz. To reflect the overall trend of the TENG output dependence on vibration frequency, average peak voltage and peak current output at each measurement point were plotted against frequency and shown in Figure 3c and d, respectively. From the results, we can see that ~100 Hz was the resonance frequency of the device and the mechanical energy was mostly effectively converted into electricity under resonance. On the other hand, the full width at half-maximum (fwhm) for voltage and current output was measured to be 127 and 102 Hz, respectively, much wider than the

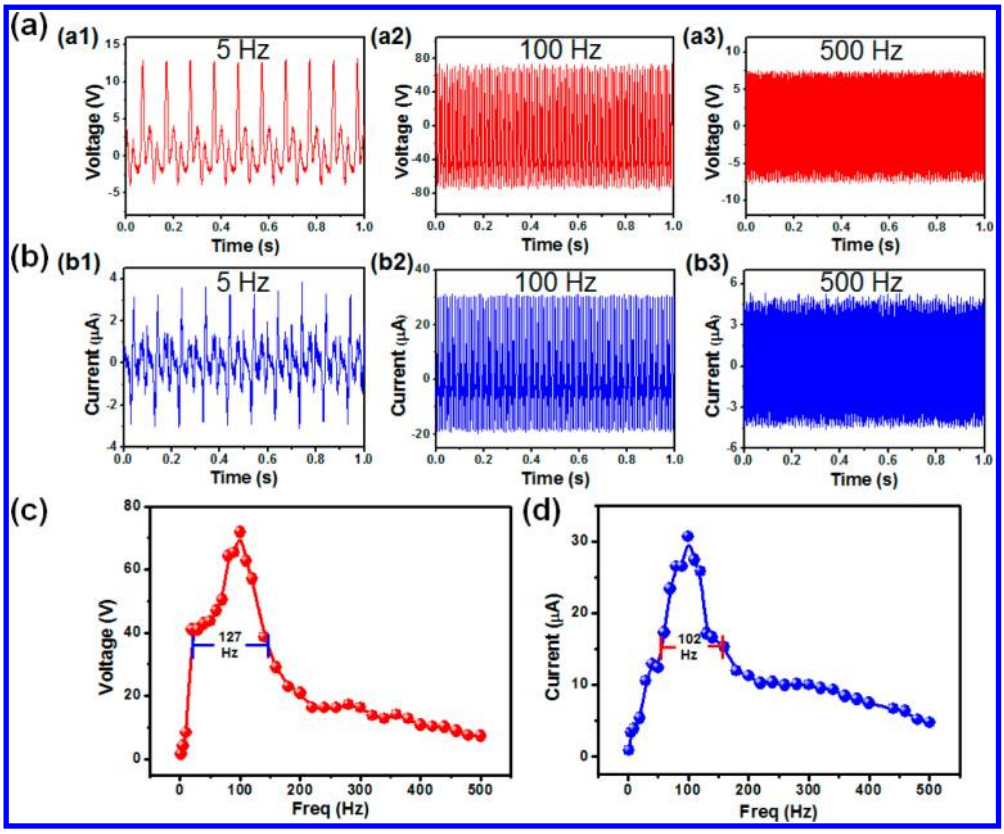

Figure 3. Measurement of the TENG's output triggered by a vibration shaker. Selected voltage output of the device at (a) (a1) 5 Hz, (a2) 100 Hz, and (a3) 500 Hz. Selected current output of the device at (b) (b1) 5 Hz, (b2) 100 Hz, and (b3) 500 Hz. (c) Peak voltage output dependence on vibration frequency. A fwhm of 127 Hz is observed. (d) Peak current output dependence on vibration frequency. A fwhm of 102 Hz is observed.

state-of-the-art vibration energy harvesters.[22,27,28] This indicates that our TENG was able to efficiently harvest mechanical energy over a broad range of frequencies. We attribute this broadband feature to two factors. First the wavy core has a changing contact area with the PTFE film during vibration, making it an imperfect spring. The other factor is the bonding electrical tape, which act as a damper for the vibration. Both bring nonlinear factors into the stiffness k of the device, which is responsible for the broader resonance bandwidth.[20−22]

To study the ability of TENG to power external loads, the device was tested at 100 Hz under variable load resistance. An adjustable resistor was used as the load, providing resistance from as low as 1 kΩ to as high as 100 MΩ. The electrometer was connected in parallel with the resistor to measure the output voltage and was connected in series with the resistor to measure the output current. Figure 4a shows average peak outputs at each resistance value and that the output voltage increases with increasing load resistance while the output current increases with decreasing load resistance. Instantaneous peak power density, calculated by $P_d = I^2R/S$, is plotted according to load resistance in Figure 4b, and the highest peak power density of 0.4 W/m^2 was obtained at the load resistance of 5 MΩ. To get a visualization of the TENG powering external loads, we connected 104 green LEDs in series with the generator mounted on the shaker, and a photograph of the experimental setup is shown in Figure 4c. By starting the shaker at a 100 Hz vibration frequency, all of the LEDs connected were simultaneously lit up, as shown in Figure 4d (see Video S1). In addition to using high-frequency sources, we also demonstrated using the TENG to collect very low frequency energy such as human body motion. As shown in Figure 4e, the device was put on the ground, covered by a piece of carpet, and also connected to the same 104 green LEDs. By simply stepping on the carpet once, all of the LEDs were simultaneously lit up, as shown in Figure 4d (see Videos S2 and S3). So far, we have demonstrated the frequency response characteristics of our TENG and the energy-harvesting ability at both low and high frequencies by lighting up LEDs.

In the following, we will focus on one issue, which is using the TENG for harvesting ocean wave energy. Restricted by our experimental conditions, we will use a bathtub to mimic the scenario. Figure 5a shows a schematic of the experiment setup. The device was sealed into a thin rubber pocket for water proofing, as shown by the inset in Figure 5a. Then the pocket was fixed to the side wall of the tub. For demonstration purposes, LEDs could be connected to the TENG; for measurement purposes, an electrometer could be

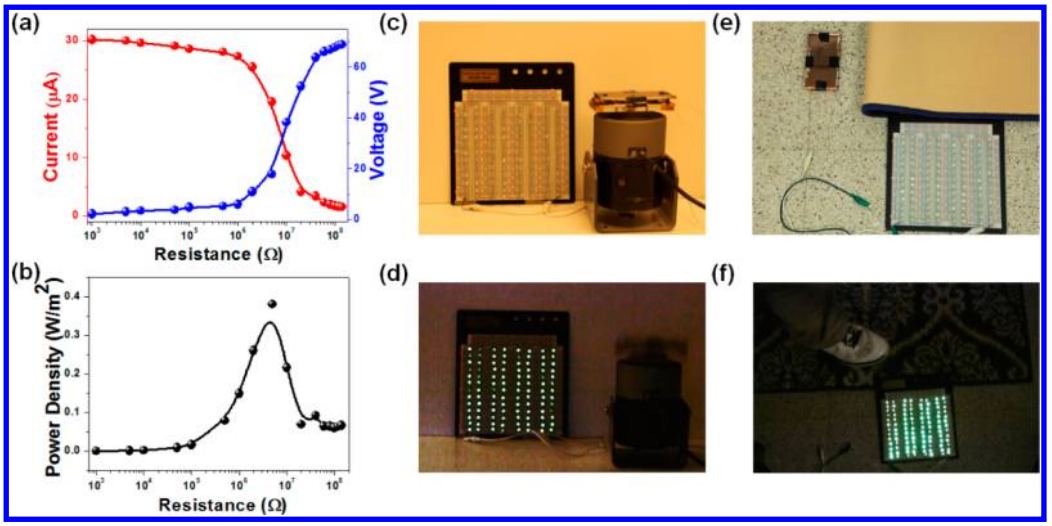

Figure 4. (a) At the vibration frequency of 100 Hz, output peak voltage and peak current dependence on load resistance. (b) At the vibration frequency of 100 Hz, output peak power density dependence on load resistance. (c) Photograph of the TENG mounted on the shaker, connected to 104 green LEDs. (d) Photograph of the 104 green LEDs lit up simultaneously by the TENG triggered by the shaker. (e) Photograph of the TENG to be covered by carpet, connected to 104 green LEDs. (f) Photograph of the 104 green LEDs lit up simultaneously by the TENG triggered by footsteps.

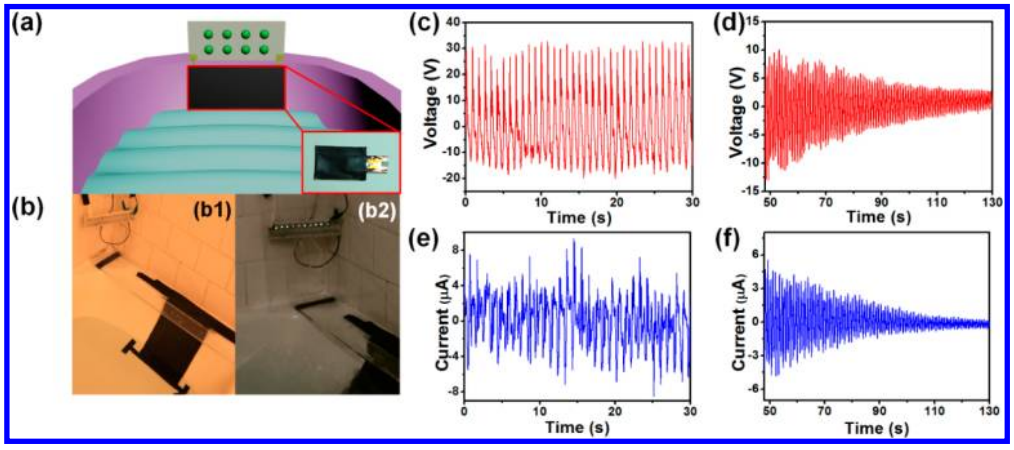

Figure 5. (a) Schematic of the experimental setup for the packaged TENG to collect water wave energy. (b) (b1) Photograph of the experimental setup for the packaged TENG to collect water wave energy; (b2) photograph of the 10 green LEDs simultaneously lit up by the TENG triggered by water waves. (c) Voltage output of the TENG triggered by water waves. (d) Damping of the voltage output after the water agitation is stopped. (e) Current output of the TENG triggered by water waves. (f) Damping of the current output after the water agitation is stopped.

connected to the TENG. Figure 5b (b1) shows the optical picture of the setup in which the TENG was connected to 10 LEDs in series. By agitating the water in the tub, waves were created that periodically impacted the device (propagating speed approximately 0.5m/s). From Figure 5b (b2) (see Video S4), we can see that the LEDs were simultaneously lit up, indicating that the TENG converted part of the mechanical energy from the water wave into electricity. Output voltage signals were subsequently captured by the electrometer, and the data are shown in Figure 5c, giving a peak voltage of ~24 V. After the removal of the agitation source, however, the water motion would not stop immediately due to the residual wave, and the TENG was also able to harvest the remaining mechanical energy. From what is shown in Figure 5d, the output voltage gradually reduced, but the TENG could still give an output of ~1.2 V after the agitation was stopped for more than 1 min. Correspondingly, the current output during agitation is shown in Figure 5e, giving a peak output of ~6 μA, and the current output after the removal of agitation is shown in Figure 5f, giving a peak output of 0.3 μA after 1 min of damping. It must be noted that the surface area of the harvesting device as well as the amount of water energy provided in our demonstration is very limited, and much more can be expected by means of increasing the device area, stacking up multilayers, and testing in real ocean waves based on our model and design.

In addition, what is equally interesting and important is to look at our experimental results from the sensor's point of view. The signals we obtain can tell us

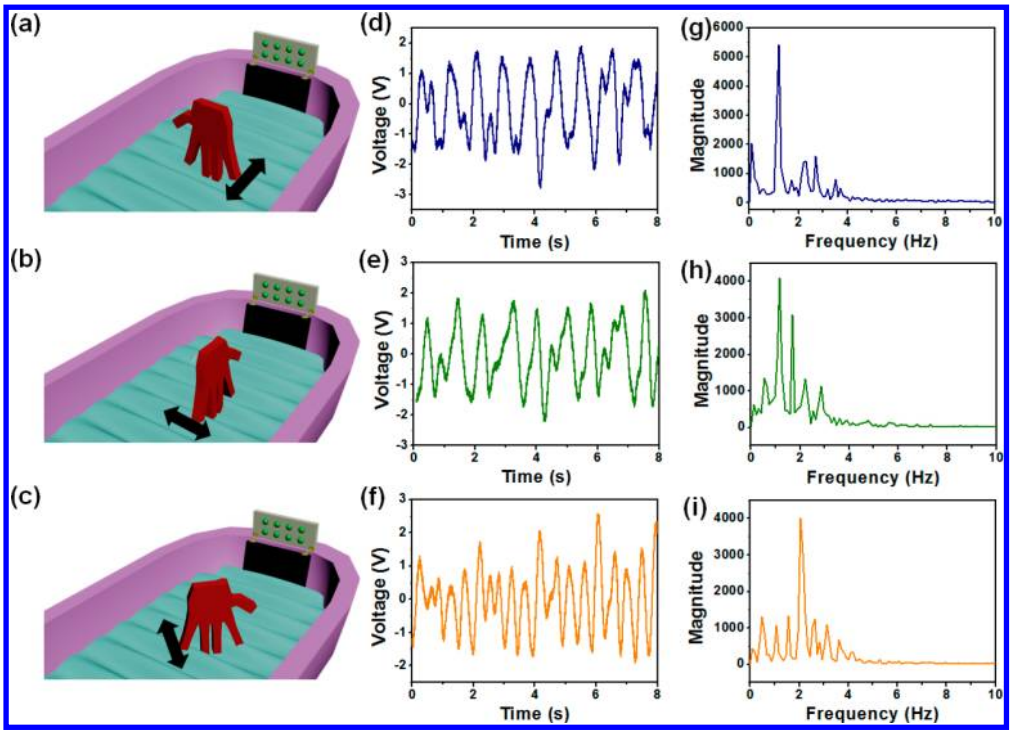

Figure 6. Three different directions of water agitation. (a) Normal to the TENG surface (case 1). (b) Parallel to the TENG surface (case 2). (c) 45° angle relative to the TENG surface (case 3). Voltage outputs of (d) case 1, (e) case 2, and (f) case 3. FFT spectra of the voltage outputs of (g) case 1, (h) case 2, and (i) case 3.

about the frequency and strength of the wave, which are important parameters in hydrological analysis. With this in mind, we went a step further to see whether more information about the state of water motion could be extracted from the output signals of our TENG. Here, we use mild agitations of the same magnitude and frequency but different directions to create water waves and study how the difference will be reflected by the output signals of the TENG. As illustrated in the schematics of Figure 6a−c, we used three different directions of agitation, one being normal to the TENG surface (case 1), one being parallel to the TENG surface (case 2), and one having a 45° angle relative to the TENG surface (case 3). Voltage output for case 1 agitation was measured and is shown in Figure 6d in navy blue color; voltage output for case 2 agitation was measured and is shown in Figure 6e in olive color; voltage output for case 3 agitation was measured and is shown in Figure 6f in orange color. The corresponding current outputs are respectively shown in Figure S1d−f. To interpret the results, let us first discuss the possible differences for the three cases. Since all of them use agitations of the same magnitude and frequency, the power input was the same. However, this does not mean the TENG will have the same output peak values and frequencies. Agitation directions will influence the propagation direction and interference pattern of the main wave and subwaves, and consequently the sequence and timing of the wave energy packets being received by the TENG are different. This will not only lead to differences in the TENG's output amplitude and frequency but also affect the details in its waveform. By comparing the outputs of case 1 and case 2, we find that they have very similar output amplitude and frequency; by comparing the outputs of case 3 with both case 1 and case 2, we find that it has a smaller output amplitude but higher output frequency. This implies that in case 3 the wave energy was split into more packets. These packets also had phase separations, reaching the TENG at different moments. Moreover, the waveforms of all three cases look different to some extent. To effectively reflect the differences in the frequency domain and reveal the details hidden in the waveforms, FFT was performed and the spectra for the voltage outputs are shown in Figure 6g−i in correspondence with Figure 6d−f, and the spectra for the current outputs are shown in Figure S1g−i in correspondence with Figure S1 d−f. By comparison, we can observe obvious differences in the number of peaks and peak positions. For example, in Figure 6g, there are sequentially one weak, two strong minor peaks to the right of the major peak and one weak, one strong minor peak to the left of the major peak; in Figure 6h, there are sequentially three strong minor peaks to the right of the major peak and one strong, one weak minor peak to the left of the major peak; in Figure 6i, there are sequentially three strong minor peaks to the right of the major peak and also three strong minor peaks to the left of the major peak. Although the three methods of agitation have the

same magnitude and frequency, by analyzing the amplitude, frequency, and FFT spectra of the output signals, we are able to identify all three cases. This demonstrates that in addition to water wave energy harvesting our TENG also has the potential for hydrological analysis, which is a very important function for a wave energy farming system.

So far, we have shown that our TENG can be used to harvest water wave energy and in the meanwhile analyze water motion. Several important advantages of TENGs over electromagnetic generators will be reiterated in the following. The first and foremost one is the extremely low cost, so that with decent investment such devices could be deployed at very large scales, onshore and offshore. With no delicate metal parts in the device, erosion from seawater can be kept at a minimal level. When necessary, replacement will also be relatively cheap. Second, the light weight of the polymeric device makes it sensitive to very slight water motions, which is important not only for scavenging small amounts of energy but also for accurately monitoring water motions even for relatively still water bodies. Third, this technology uses readily available materials and simple manufacturing processes. Thus, there is little barrier for the industry to set up manufacturing plants, which further reduces the time and money needed to push forward the commercialization of TENGs. Last but not least, the major component for ocean wave harvesting is the offshore wind power. Interestingly as demonstrated by previous works,[29,30] the TENG is also proved to be very suitable for wind power harvesting. This means that the two competing schemes can be combined together to potentially provide sufficient green energy to the coast line and even in-land inhabitants.

CONCLUSION

In summary, we invented an innovative triboelectric nanogenerator that is based on a wavy-structured Cu−Kapton−Cu film sandwiched between two flat nanostructured PTFE films for specifically harvesting energy due to mechanical vibration/impacting/compressing using the triboelectrification effect. This structure design allows the TENG to be self-restorable after impact without the use of extra springs and also converts direct impact into lateral sliding, which is proved to be a much more efficient friction mode for energy harvesting. The working mechanism has been elaborated using the capacitor model and finite-element simulation. Vibrational energy from 5 to 500 Hz has been harvested, and the generator's resonance frequency was determined to be ~100 Hz at a broad fwhm of over 100 Hz, producing an open-circuit voltage of up to 72 V, a short-circuit current of up to 32 μA, and a peak power density of 0.4 W/m^2. Most importantly, the wavy structure of the TENG can be easily packaged so that there is no infiltration of water or air, and it can be adequately applied to harvest the impact energy from water waves, clearly establishing the principle for ocean wave energy harvesting. Lastly, different ways of water agitation were studied to trigger the packaged TENG. By analyzing the output signals and their corresponding FFT spectra, three methods of agitation were distinguished from each other, demonstrating the potential of the TENG for hydrological analysis. Considering the unique advantages of TENGs, such as cost-effectiveness, light weight, and easy scalability, this approach might open the possibility for obtaining green and sustainable energy from the ocean using nanostructured materials.

METHODS

Raw materials for fabricating the TENG include 125 μm thick Kapton film, 125 μm thick PTFE film, and 1/16 in. thick acrylic substrates and copper. First, the Kapton film was periodically bent into a wavy shape by using a set of metal rods (with diameter of 1/4 in.). Then the set was sent into a muffle oven and baked at 360 °C for 4 h. Since Kapton film is thermoplastic, it will remain in the wavy shape stably below its glass transition temperature.[31,32] Then 200 nm copper was sputtered on both sides of the wavy Kapton film as electrodes. Second, two slides of PTFE films were prepared by applying ICP etching[23,24] (specifically 15 sccm Ar, 10 sccm O_2, and 30 sccm CF_4 under 400 W RF power and 100 W bias power) on one side of the films, and nanostructures were thus obtained, which will largely enhance contact electrification.[18,25,26] Then, 200 nm thick copper was subsequently sputtered on the other side of the film, acting as electrodes. The copper side of the PTFE films was then tightly adhered to two acrylic substrates respectively by using a thin layer of cured PDMS. By sandwiching the Cu−Kapton−Cu wavy core using the two acrylic substrates with PTFE films facing inside and bonding the structures together with electrical tape, the final device structure is obtained.

Conflict of Interest: The authors declare no competing financial interest.

Acknowledgment. The research was supported by MURI, DOE, the "Thousands Talents" Program for Pioneer Researcher and His Innovation Team, China, and the Beijing City Committee of Science and Technology Project (Z131100006013004, Z131100006013005).

Supporting Information Available: Additional figure of the current output part of the water motion analysis and additional demonstration videos of the TENG lighting up LEDs driven by the shaker, footsteps, and water waves are available free of charge *via* the Internet at http://pubs.acs.org.

REFERENCES AND NOTES

1. Brown, K. S. Bright Future - or Brief Flare - for Renewable Energy? *Science* **1999**, *285*, 678–680.
2. Clery, D. Renewable Energy - U. K. Ponders World's Biggest Tidal Power Scheme. *Science* **2008**, *320*, 1574–1574.
3. Glaser, J. A. US Renewable Energy Consumption. *Clean Technol. Environ.* **2007**, *9*, 249–252.

4. Henniker, J. Triboelectricity in Polymers. *Nature* **1962**, *196*, 474.
5. Wang, Z. L. Triboelectric Nanogenerators as New Energy Technology for Self-Powered Systems and as Active Mechanical and Chemical Sensors. *ACS Nano* **2013**, *7*, 9533–9557.
6. Davies, D. K. Charge Generation on Dielectric Surfaces. *J. Phys. D Appl. Phys.* **1969**, *2*, 1533–1537.
7. Marshall, A. W. *The "Wimshurst" Machine, How to Make and Use It*; Spon and Chamberlain: New York, 1908.
8. Dorf, R. C. *The Electrical Engineering Handbook*; CRC Press: Boca Raton, FL, 1993.
9. Fan, F. R.; Tian, Z. Q.; Wang, Z. L. Flexible Triboelectric Generator!. *Nano Energy* **2012**, *1*, 328–334.
10. Wang, S. H.; Lin, L.; Wang, Z. L. Nanoscale Triboelectric-Effect-Enabled Energy Conversion for Sustainably Powering Portable Electronics. *Nano Lett.* **2012**, *12*, 6339–6346.
11. Fan, F. R.; Lin, L.; Zhu, G.; Wu, W. Z.; Zhang, R.; Wang, Z. L. Transparent Triboelectric Nanogenerators and Self-Powered Pressure Sensors Based on Micropatterned Plastic Films. *Nano Lett.* **2012**, *12*, 3109–3114.
12. Wen, X. N.; Su, Y. J.; Yang, Y.; Zhang, H. L.; Wang, Z. L. Applicability of Triboelectric Generator over a Wide Range of Temperature. *Nano Energy* **2014**, *4*, 150–156.
13. Cruz, J. *Ocean Wave Energy: Current Status and Future Prepectives* [i.e. perspectives]; Springer: Berlin, 2008.
14. U.S. Department of the Interior. *Technology White Paper on Wave Energy Potential on the U.S. Outer Continental Shelf*; U.S. Dept. of the Interior Minerals Management Service Renewable Energy and Alternate Use Program: Washington, D.C., **2006**. http://purl.access.gpo.gov/GPO/LPS94821.
15. Electric Power Research Institute. *Mapping and Assessment of the United States Ocean Wave Energy Resource*; Final report; EPRI Electric Power Research Institute: Palo Alto, CA, **2011**; p 1 online resource.
16. American Wind Energy Association, United States Department of Energy. *Inventory of State Incentives for Wind Energy in the U.S.: a State by State Survey*; American Wind Energy Association: Washington, D.C., **2001**; http://www.awea.org/policy/documents/inventory.pdf.
17. Global Wind Energy Council. *Global Wind Report Annual Market Update 2012*; 2012; http://www.gwec.net/wp-content/uploads/2012/06/Annual_report_2012_LowRes.pdf.
18. Wang, S. H.; Lin, L.; Xie, Y. N.; Jing, Q. S.; Niu, S. M.; Wang, Z. L. Sliding-Triboelectric Nanogenerators Based on In-Plane Charge-Separation Mechanism. *Nano Lett.* **2013**, *13*, 2226–2233.
19. Zhu, G.; Chen, J.; Liu, Y.; Bai, P.; Zhou, Y. S.; Jing, Q. S.; Pan, C. F.; Wang, Z. L. Linear-Grating Triboelectric Generator Based on Sliding Electrification. *Nano Lett.* **2013**, *13*, 2282–2289.
20. Hajati, A.; Kim, S. G. Ultra-wide Bandwidth Piezoelectric Energy Harvesting. *Appl. Phys. Lett.* **2011**, *99*, 083105.
21. Tang, L. H.; Yang, Y. W.; Soh, C. K. Toward Broadband Vibration-Based Energy Harvesting. *J. Intell. Mater. Syst. Struct.* **2010**, *21*, 1867–1897.
22. Zhu, D. B.; Tudor, M. J.; Beeby, S. P. Strategies for Increasing the Operating Frequency Range of Vibration Energy Harvesters: A Review. *Meas. Sci. Technol.* **2010**, *21*, 022001.
23. Morber, J. R.; Wang, X. D.; Liu, J.; Snyder, R. L.; Wang, Z. L. Wafer-Level Patterned and Aligned Polymer Nanowire/Micro- and Nanotube Arrays on any Substrate. *Adv. Mater.* **2009**, *21*, 2072–2076.
24. Fang, H.; Wu, W. Z.; Song, J. H.; Wang, Z. L. Controlled Growth of Aligned Polymer Nanowires. *J. Phys. Chem. C* **2009**, *113*, 16571–16574.
25. Yang, W. Q.; Chen, J.; Zhu, G.; Wen, X. N.; Bai, P.; Su, Y. J.; Lin, Y.; Wang, Z. L. Harvesting Vibration Energy by a Triple-Cantilever Based Triboelectric Nanogenerator. *Nano Res.* **2013**, *6*, 880–886.
26. Yang, Y.; Zhang, H. L.; Chen, J.; Jing, Q. S.; Zhou, Y. S.; Wen, X. N.; Wang, Z. L. Single-Electrode-Based Sliding Triboelectric Nanogenerator for Self-Powered Displacement Vector Sensor System. *ACS Nano* **2013**, *7*, 7342–7351.
27. Beeby, S. P.; Tudor, M. J.; White, N. M. Energy Harvesting Vibration Sources for Microsystems Applications. *Meas. Sci. Technol.* **2006**, *17*, R175–R195.
28. Anton, S. R.; Sodano, H. A. A Review of Power Harvesting Using Piezoelectric Materials (2003−2006). *Smart Mater. Struct.* **2007**, *16*, R1–R21.
29. Yang, Y.; Zhu, G.; Zhang, H. L.; Chen, J.; Zhong, X. D.; Lin, Z. H.; Su, Y. J.; Bai, P.; Wen, X. N.; Wang, Z. L. Triboelectric Nanogenerator for Harvesting Wind Energy and as Self-Powered Wind Vector Sensor System. *ACS Nano* **2013**, *7*, 9461–9468.
30. Xie, Y. N.; Wang, S. H.; Lin, L.; Jing, Q. S.; Lin, Z. H.; Niu, S. M.; Wu, Z. Y.; Wang, Z. L. Rotary Triboelectric Nanogenerator Based on a Hybridized Mechanism for Harvesting Wind Energy. *ACS Nano* **2013**, *7*, 7119–7125.
31. DuPont. DuPont Kapton HN polyimide film.
32. Baeurle, S. A.; Hotta, A.; Gusev, A. A. On the Glassy State of Multiphase and Pure Polymer Materials. *Polymer* **2006**, *47*, 6243–6253.